Contents lists available at ScienceDirect

Nuclear Instruments and Methods in Physics Research A

journal homepage: www.elsevier.com/locate/nima

Probing active-edge silicon sensors using a high precision telescope

K. Akiba [a], M. Artuso [b], V. van Beveren [c], M. van Beuzekom [c], H. Boterenbrood [c], J. Buytaert [d], P. Collins [d], R. Dumps [d], B. van der Heijden [c], C. Hombach [e], D. Hynds [f], D. Hsu [b], M. John [h], E. Koffeman [c], A. Leflat [i], Y. Li [j], I. Longstaff [f], A. Morton [f], E. Pérez Trigo [g], R. Plackett [k], M.M. Reid [l], P. Rodríguez Perez [e], H. Schindler [d], P. Tsopelas [c,*], C. Vázquez Sierra [g], M. Wysokiński [m]

[a] Federal University of Rio de Janeiro, Rio de Janeiro, Brazil
[b] Syracuse University, Syracuse, NY, United States
[c] Nikhef, Amsterdam, Netherlands
[d] CERN, the European Organisation for Nuclear Research, Geneva, Switzerland
[e] University of Manchester, Manchester, Lancashire, UK
[f] Glasgow University, Glasgow, Lanarkshire, UK
[g] Universidade de Santiago de Compostela, Santiago de Compostela, Spain
[h] University of Oxford, Oxfordshire, UK
[i] Lomonosov Moscow State University, Moscow, Russia
[j] Tsinghua University, Beijing, China
[k] Diamond Light Source Ltd., Didcot, Oxfordshire, UK
[l] University of Warwick, Coventry, UK
[m] AGH University of Science and Technology, Krakow, Poland

ARTICLE INFO

ABSTRACT

The performance of prototype active-edge VTT sensors bump-bonded to the Timepix ASIC is presented. Non-irradiated sensors of thicknesses 100–200 μm and pixel-to-edge distances of 50 μm and 100 μm were probed with a beam of charged hadrons with sub-pixel precision using the Timepix telescope assembled at the SPS at CERN. The sensors are shown to be highly efficient up to a few micrometers from the physical edge of the sensor. The distortion of the electric field lines at the edge of the sensors is studied by reconstructing the streamlines of the electric field using two-pixel clusters. These results are supported by TCAD simulations. The reconstructed streamlines are used to study the field distortion as a function of the bias voltage and to apply corrections to the cluster positions at the edge.
© 2014 CERN for the benefit of the Authors. Published by Elsevier B.V. This is an open access article under the CC BY license (http://creativecommons.org/licenses/by/4.0/).

1. Introduction

Silicon pixel detectors are chosen in experiments where radiation hardness and high precision tracking are demanded. In order to cover a large detection area, the tiling of many sensors is necessary. Conventional sensors use guard ring electrodes to gradually reduce the electric field towards the edge and in this way isolate the pixel matrix from edge effects. However, this results in an area with reduced sensitivity at the edge of the sensor up to a few hundred microns. In recent years, novel types of sensors with a smaller inactive area at the edge have been developed. These so-called edgeless sensors are divided into two sub-categories, slim-edge and active-edge. In the case of slim-edge sensors the sensor is diced and passivated closer to the pixel matrix [1] while in the case of the active-edge [2] the sensor is etched and doped[1] [3]. The presence of this doping layer suppresses the surface current between electrodes but also distorts the electric field at the edge of the sensor. In this paper the performance at the edge of a series of non-irradiated active-edge sensors manufactured by VTT[2] is studied.

2. Experimental setup

As part of the LHCb VELO upgrade programme, a high efficiency telescope had been assembled in the SPS North Area at CERN. The telescope [4] consisted of eight Timepix [5] detectors with 300 μm

---

[1] The implant type at the edge depends on the sensor type: n^+ edge for a p-on-x sensor and p^+ edge for a n-on-x where x is either n or p.
[2] VTT Technical Research Centre of Finland P.O. Box 5520 FI-01051 LASKUT Finland.

* Corresponding author.

Table 1
A list of the VTT sensors tested.

Timepix chip	Sensor type	Thickness (μm)	PTE (μm)	Full depletion voltage (V)	Guard ring	Interpixel isolation[a]	Bias voltage (V)
D07-W0160	n-on-n	150	50	7–10	No	p-Stop	−40, −20
J08-W0171	n-on-p	100	50	10–13	No	p-Spray	−60
F08-W0171	n-on-n	200	50	14–17	No	p-Spray	−60
C07-W0171	n-on-p	100	100	10–13	No	p-Spray	−80
H08-W0171	n-on-n	200	100	14–17	Floating[b]	p-spray	−80, −40

[a] A p-type implant is needed between the pixels of an n-on-x sensor to interrupt the electron layer formed below the oxide.
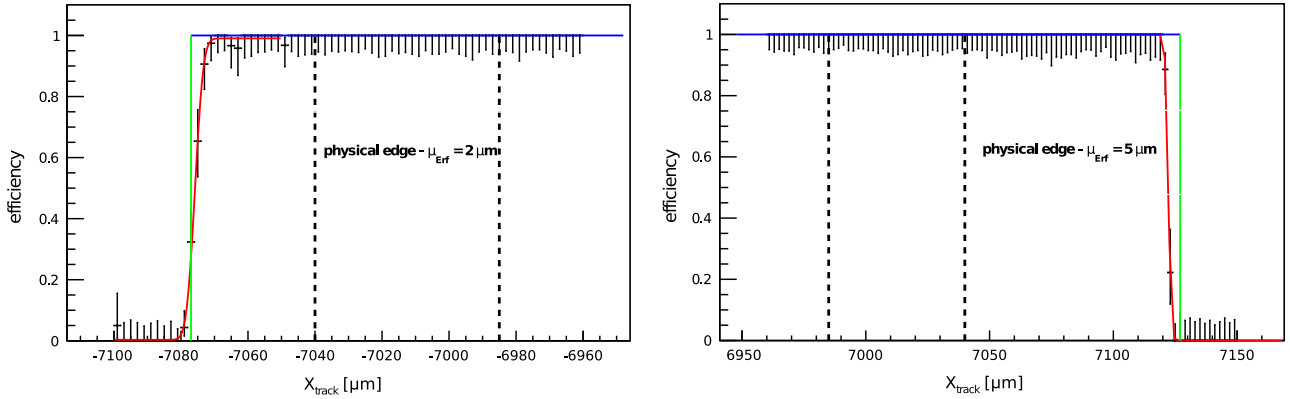[b] A floating guard ring is a guard ring that is not grounded.

Fig. 1. Efficiency at the side edge of the 150 μm thick n-on-n sensor D07-W0160 with 50 μm PTE (left) and at the side edge of the 100 μm thick n-on-p sensor C07-W0171 with 100 μm PTE (right). The dashed lines represent the boundaries of the last pixel, the (green) vertical line represents the physical edge and the (blue) horizontal line indicates the maximum efficiency. The legend states the distance between the mean of the error function and the physical edge. (For interpretation of the references to color in this figure caption, the reader is referred to the web version of this paper.)
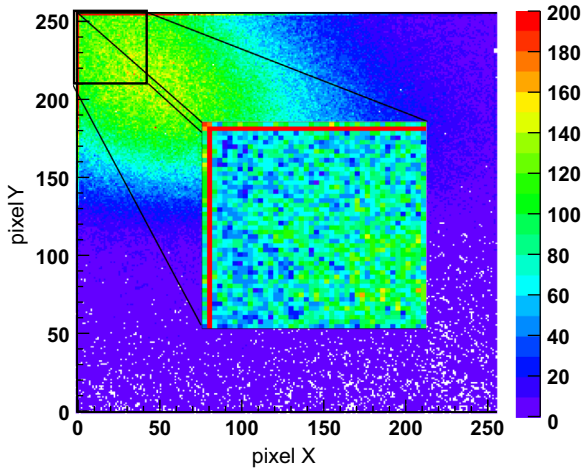

Fig. 2. Hit map of the 150 μm thick n-on-n sensor D07-W0160 with 50 μm PTE. A "hot" column and row (shown in the zoomed picture) second to the last ones are the results of the distortion of the electric field pattern at the edge.

thick sensors equally divided into two arms with an additional ninth plane providing timing information. The device under test (DUT) was mounted on a computer controlled translation and rotation stage which allowed translations in transverse directions to the beam in steps of 1 μm, as well as 0.01 of a degree accurate rotations. The stage was placed between the two telescope arms where the track pointing resolution is less than 2 μm. A series of prototype active-edge sensors from VTT of thicknesses 100–200 μm, pixel-to-edge (PTE) distances of 50 μm and 100 μm and different sensor types (n-on-n and n-on-p) were bump-bonded on Timepix chips and installed as DUTs in the Timepix telescope. The PTE is defined as the distance from the edge of the last pixel implant to the cut edge. All sensors have a pixel pitch of 55 μm. The pixel implants are

circular with a diameter of 28 μm. The sensor of one of the DUTs (H08-W0171) has one guard ring with a width of 11 μm. Metrology results indicate that the sensor size and alignment with respect to the readout ASIC are in agreement with the values from the design. A list of the five sensors and their properties is presented in Table 1.

The center of the beam spot was aligned with the edge of the sensors in order to acquire higher statistics for this sensor region. The beam consisted of charged hadrons with a momentum of 180 GeV/c. All data shown in this paper were taken with the DUT orientated perpendicular to the beam axis. Runs at different bias voltages were taken for a selection of these sensors.

3. Determination of hit position

The tracks are reconstructed and fitted using only hits on the telescope planes in order to avoid biasing of the results. The fitted track from the telescope is extrapolated to the position of the DUT to predict the intercept point of the track on the DUT. The track selection cut is an upper cut in the χ^2 probability of 0.5%. The surviving tracks are used to align the telescope planes and subsequently the DUT. The telescope planes are tilted to 9° to achieve the optimum spatial resolution [6]. The residuals (defined as the X (Y) predicted by the telescope minus the X (Y) of the cluster) have a σ of 3–5 μm for the telescope planes and 9–12 μm for the DUTs depending on the bias voltage supplied and the thickness of the sensor. The smaller residuals are a result of setting the telescope planes in their optimum angle in contrast to the DUT which is set perpendicular to the beam. The telescope and the DUT planes are lying on the XY plane where the column number of the pixel matrix corresponds to the X-axis and the row number to the Y-axis. A local coordinate system (X,Y) is defined with the (0,0) set at the center of the pixel matrix.
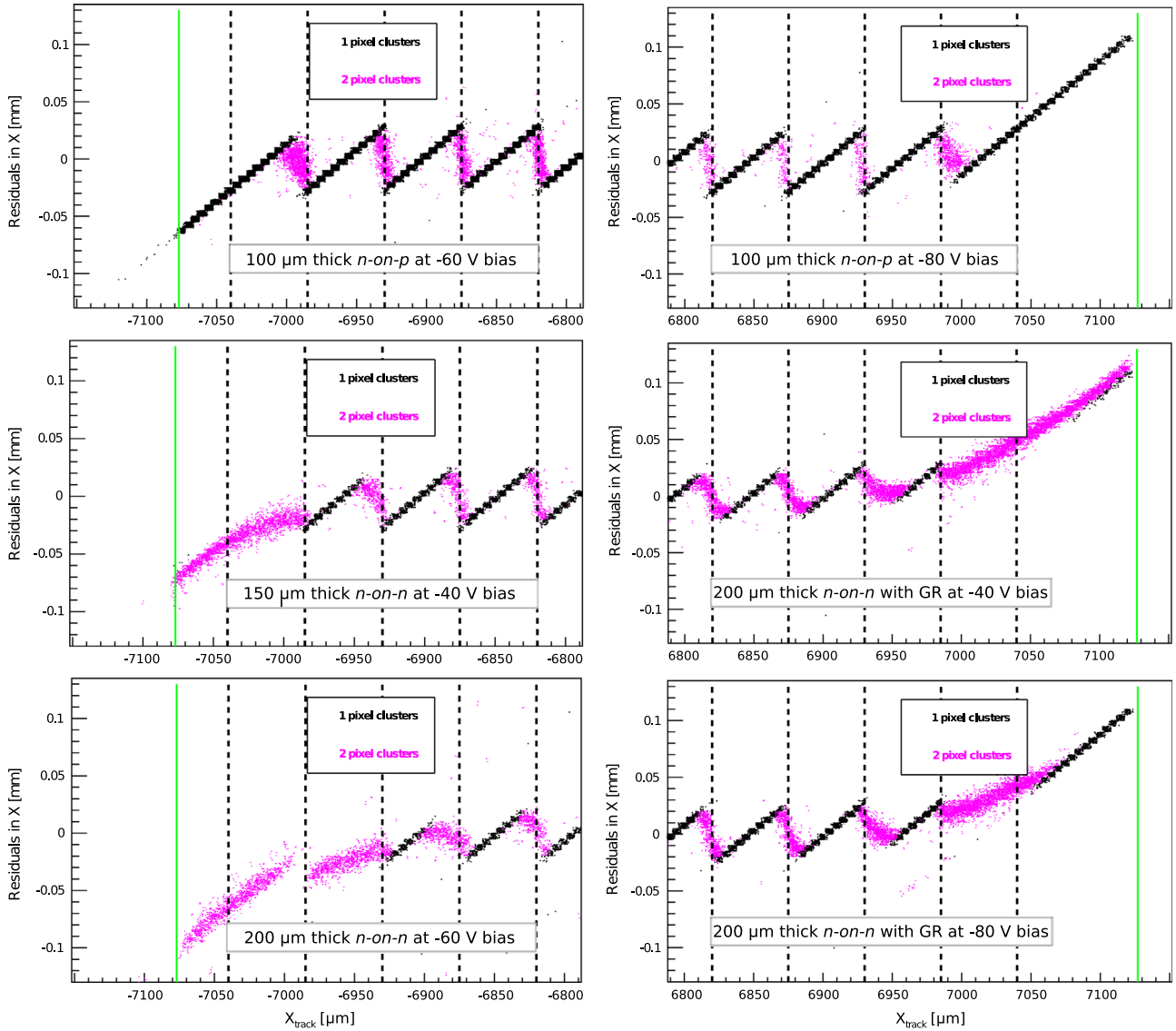
Fig. 3. Residuals in X as a function of the X coordinate predicted by the telescope for the sensors with 50 μm PTE (left column) and 100 μm PTE (right column): 100 μm thick n-on-p J08-W0171 at -60 V bias (top left), 150 μm thick n-on-n D07-W0160 at -40 V bias (middle left), 200 μm thick n-on-n F08-W0171 at -60 V bias (bottom left), 100 μm thick n-on-p C07-W0171 at -80 V bias (top right), 200 μm thick n-on-n H08-W0171 at -40 V bias (middle right) and at -80 V bias (bottom right). The dotted lines represent the pixel boundaries and the green line the physical edge. The absence of hits in the boundary between the last two pixels of the 200 μm thick n-on-n sensor F08-W0171 (bottom left) is due to the appearance of three-pixel clusters and is discussed in Section 6. (For interpretation of the references to color in this figure caption, the reader is referred to the web version of this paper.)

All the DUTs were operated in Time-over-Threshold (ToT) mode. In ToT mode, for each pixel hit a counter is incremented for as long as the preamplifier output is above threshold, thereby giving a measurement of the energy deposited in this pixel. The counting clock had a frequency of 40 MHz. For a minimum ionizing particle (MIP) traversing the 150 μm thick n-on-n sensor (D07-W0160), the most probable value is 150 ToT counts when collecting electrons. The most probable ToT value depends on the thickness, type and polarity of the sensor. The ToT counts provided by the pixels are then converted into charge by applying a surrogate function [6] with different fit parameters for each device obtained from testpulse data. The center position of the cluster is calculated by using the center of gravity (CoG) method.[3] For

clusters containing edge pixels, the CoG method does not provide accurate information about the track position causing a divergence from zero in the residual distributions as will be described in Section 5.

4. Efficiency towards the physical edge

To measure the efficiency (defined as the ratio of number of tracks with a matching cluster on the DUT over the number of tracks predicted by the telescope) the following procedure is used:

(*footnote continued*)
charge calibration correction with the formula

$$x_{COG} = x_0 + \frac{\sum_{i=0}^{N} x_i q_i}{\sum_{i=0}^{N} q_i}$$

---

[3] In the center of gravity method the position of the hit on N pixels is calculated after weighting the position of the pixels using their respective charge after the
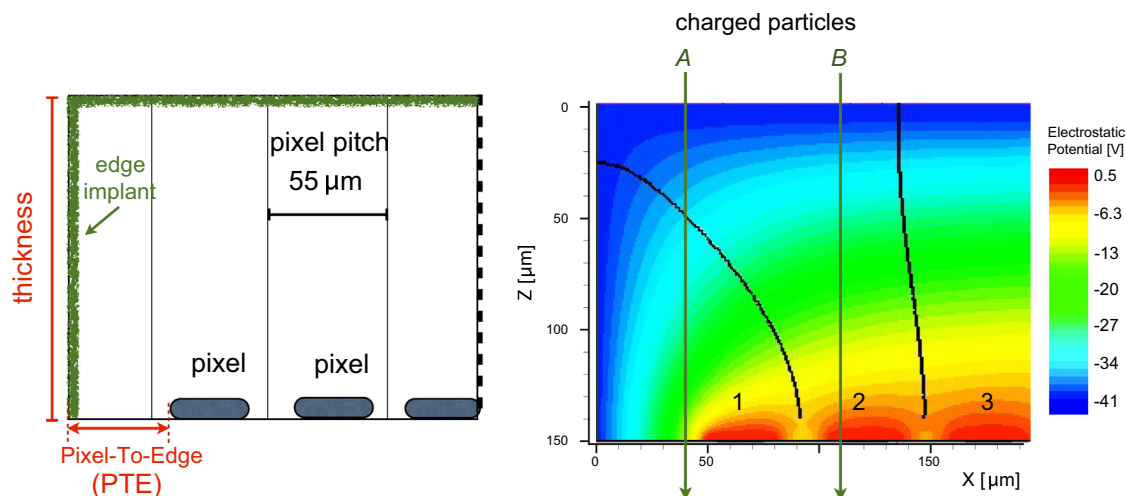
Fig. 4. *Left*: Anatomy of an active-edge sensor. Figure not to scale. *Right*: TCAD simulation of the electrostatic potential of a 150 μm thick n-on-n sensor with 50 μm PTE, *p*-stop interpixel isolation operating at −40 V. The streamlines of the electric field at the edge are not perpendicular to the sensor.

a track is declared as *found* when a pixel is hit in a square window of 110 μm (two pixel pitch wide) around the telescope's prediction on the DUT. Since the pointing resolution is below 2 μm, it is possible to probe the efficiency at the edge in detail. The results are shown in Fig. 1 for the 150 μm thick n-on-n sensor (left) and the 100 μm thick n-on-p sensor (right). The efficiency distributions of all sensors with 50 μm PTE are identical to Fig. 1 (left) and the distributions for all sensors with 100 μm PTE are identical to Fig. 1 (right). The (green) vertical line represents the physical edge and the dashed lines represent the boundaries of the last pixel. The dashed lines are fixed by aligning to the pattern of one-pixel clusters within the main body of the pixel array. The position of the physical edge is defined by the PTE and verified by metrology in the case of the 150 μm thick sensor (D07-W0160). Metrology was performed at CERN using the optical measuring system MAHR Wegu OMS 600 with an uncertainty of ± 1 μm. The distance between the physical edge and the boundary of the last pixel is 37 μm for the 50 μm PTE sensors and 87 μm for the 100 μm PTE sensors. The DUTs are ∼ 100% efficient through all the pixel matrix. At the edge of the sensor, the efficiency is > 99% up to 10 μm from the physical edge. The efficiency distribution is fitted with an error function. The mean of the fitted error function is 2–7 μm away from the physical edge.

5. Residuals at the physical edge

Looking at the raw data and the integrated hit map in Fig. 2, the pixels of the second but last row (column) of some of the sensors of Table 1 show an excess of hits compared to their neighboring pixels. In those sensors it is never the case that a pixel hit is seen in the last row (column) which does not share charge with the neighboring row (column). To understand this effect the residuals at the edge were studied.

Clusters with a size larger than one are formed due to charge sharing if tracks intercept close to the boundaries of the pixel cell. In Fig. 3 the one-pixel and two-pixel cluster residuals are plotted as a function of the *X* coordinate of the track intercept as predicted by the telescope. The dotted vertical lines represent the pixel boundaries and the solid (green) vertical line represents the physical edge of the sensor. The requirement for all two-pixel clusters used in this analysis is that both pixels belong to the same row. The first and last five rows are excluded to avoid influences from the corners of the sensors. The increased rate of two-pixel clusters with respect to the center of the pixel matrix and the

absence of one-pixel clusters from the last pixel up to the physical edge are indications of the distorted pattern of the electric field. This electric field distortion at the edge depends on the thickness of the sensor, the PTE and the bias voltage applied. The dependence on the thickness and the PTE is studied in Section 6 and the dependence on the bias voltage in Section 7.

A previous paper [7] reports a distorted pattern of the electric field lines at the last columns (rows) of active-edge sensors.[4] Looking at the cross-section of such an active-edge sensor in TCAD simulations [8] we can visualize this distortion of the electric field pattern. The PTE distance and the edge implant are depicted in Fig. 4 (left). In Fig. 4 (right) the electrostatic potential of a 150 μm thick active-edge sensor with a 50 μm PTE, *p*-stop interpixel isolation operating at −40 V is simulated. In a homogeneous electric field the field lines are perpendicular between the top and bottom contact of the sensor. However, the field line at the boundary of the two edge pixels, which will be referred to as streamline, is shaped in such a way that it reduces the volume of the sensor where free charge carriers will be collected by the last pixel. Simultaneously, this effective volume[5] is increased for the one but last pixel.

For a charged particle, free charge carriers will be liberated along the whole path of the particle through the sensor (Fig. 4 right). In the case of particle *B*, all electric field lines originating from a point along the particle's trajectory end on pixel 2. However, when a particle traverses the sensor close to the edge (particle *A*) where the streamlines are curved, both the last and one but last pixel (pixels 1 and 2) collect charge. Reconstructing the edge streamline and estimating the effective volume of the edge pixels are the main topics of Section 6.

6. Charge fraction of the edge pixels

The ratio of the charge of a pixel over the total charge of the cluster can be used to estimate the effective volume of each pixel. In Fig. 5 the CoG of the two-pixel clusters as a function of the prediction from the telescope for the *X* coordinate are plotted.[6] The empty space between the charge ratio curves represents areas where the liberated charge is not shared between pixels. A particle

---

[4] In [7] the sensors are placed at large angles with respect to the beam. No telescope is used to define the intercept of a particle on the sensor.

[5] The term effective volume refers to the volume formed by the streamlines.

[6] In Figs. 5 and 6 the charge fraction is defined as the charge of the pixel closest to the edge (outer pixel) over the total charge of the two-pixel cluster it belongs to.
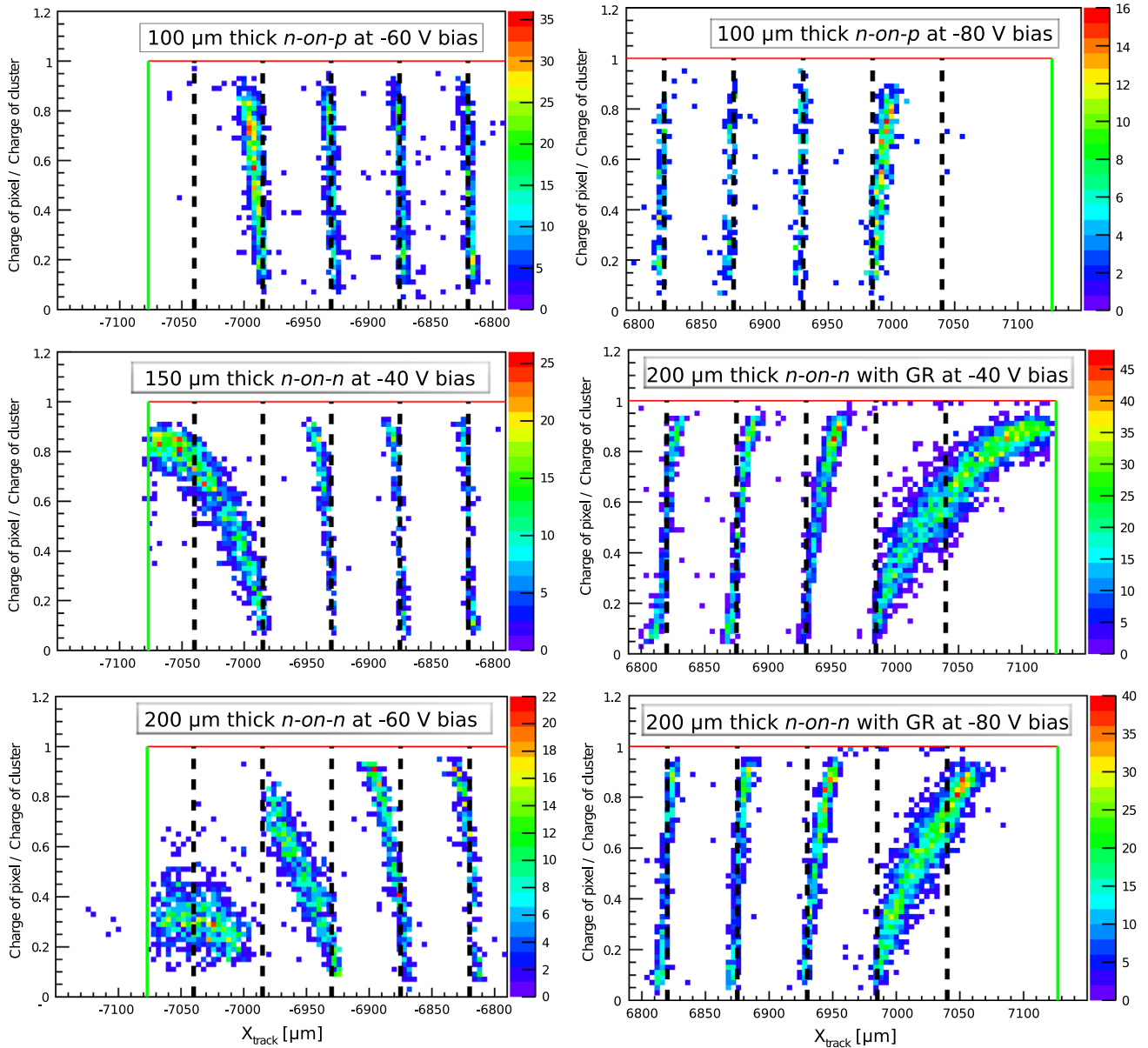
Fig. 5. Charge fractions of pixels forming two-pixel clusters at the edge of the sensors with 50 μm PTE (left column) and 100 μm PTE (right column): 100 μm thick n-on-p J08-W0171 at −60 V bias (top left), 150 μm thick n-on-n D07-W0160 at −40 V bias (middle left), 200 μm thick n-on-n F08-W0171 at −60 V bias (bottom left), 100 μm thick n-on-p C07-W0171 at −80 V bias (top right), 200 μm thick n-on-n H08-W0171 at −40 V bias (middle right) and at −80 V bias (bottom right). The dotted lines represent the pixel boundaries and the green line the physical edge. (For interpretation of the references to color in this figure caption, the reader is referred to the web version of this paper.)

traversing the sensor at a region corresponding to such an empty space will form a one-pixel cluster. For the 150 μm thick sensor with 50 μm PTE (D07-W0160) at −40 V bias the effective volume of the second to last pixel is ∼1.7 times larger[7] compared to the volume of a more central pixel while the effective volume of the last pixel (extending up to the physical edge of the sensor) is approximately the same as the volume of a more central pixel. Note that all sensors were operated at a voltage larger than the full depletion voltage, as listed in Table 1. The cluster-charge distribution (Landau) of each sensor has been compared to that expected for a fully depleted sensor and found to be in accordance to expectation. This provides an independent cross-check that the sensors were fully depleted.

The effect of the curved streamlines at the edge is also present in the case of the 200 μm thick sensor with the same PTE (F08-W0171)

at −60 V bias as shown in Fig. 6. In the region located at the boundary of the last and one but last pixel marked with the (red) dotted ellipse, three-pixel clusters with all three pixels in the same row are formed. The additional appearance of three-pixel clusters at the rows close to the edge of the 200 μm thick sensor is evidence of an even more distorted electric field than in the case of the 150 μm thick one.

The electric field pattern at the edge is less distorted in the case of J08-W0171 and C07-W0171. Fig. 5 (top left) and (top right) shows that the field lines at the pixel boundaries are uniform up to the edge of J08-W0171 and C07-W0171 respectively. Both J08-W0171 and C07-W0171 are 100 μm thick and were operated at −60 V and −80 V respectively.

The amount of distortion depends on the thickness and the PTE. For the sensors of Table 1 without guard ring we observe a reduction of the distortion as the dimensionless ratio of thickness over PTE decreases. The distortion becomes negligible when the ratio approaches one. This dependence of the electric field on the geometrical features of the sensor is expected since for a small thickness over PTE ratio the sensor

---

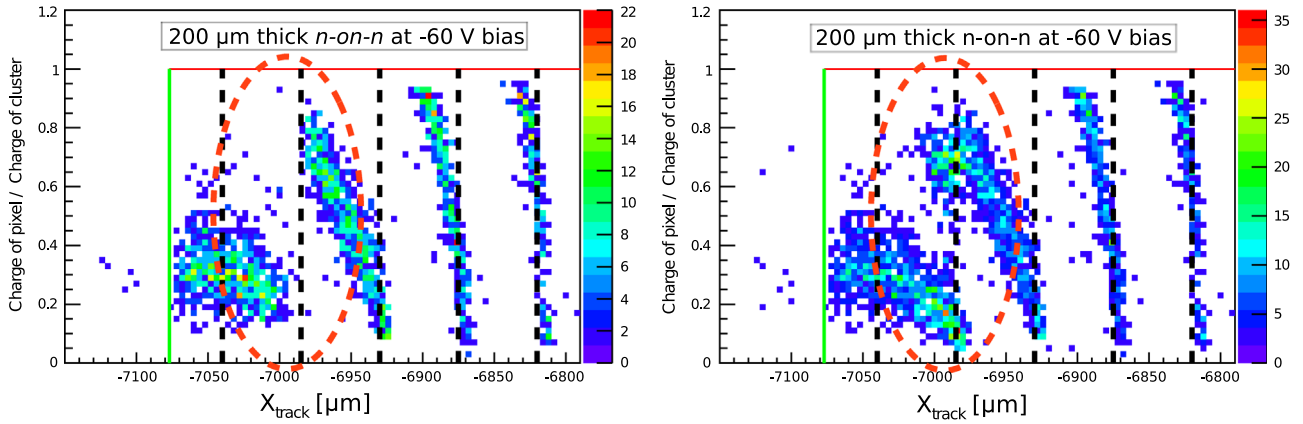[7] This value is calculated from the testbeam data.

Fig. 6. Charge fractions of pixels forming two-pixel clusters (left) and two and three-pixel clusters (right) at the side edge of the 200 μm n-on-n sensor F08-W0171 with 50 μm PTE showing a greater distortion than Fig. 5. (For interpretation of the references to color in this figure caption, the reader is referred to the web version of this paper.)
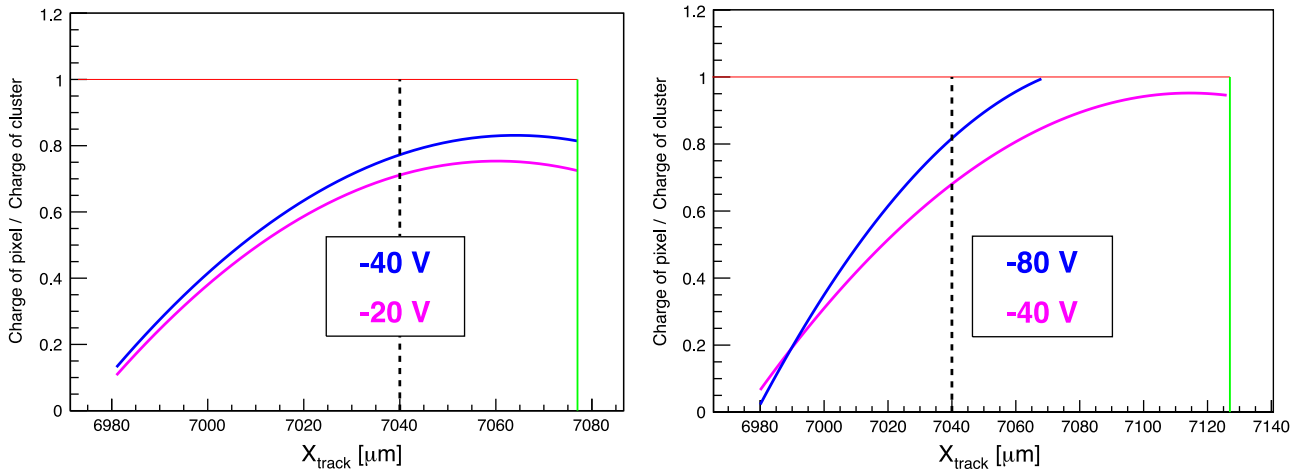

Fig. 7. Measured stream lines at the edge of the 150 μm thick n-on-n sensor D07-W0160 with 50 μm PTE (left) and the 200 μm thick n-on-n H08-W0171 with 100 μm PTE and floating GR (right) at different bias voltages. (For interpretation of the references to color in this figure caption, the reader is referred to the web version of this paper.)
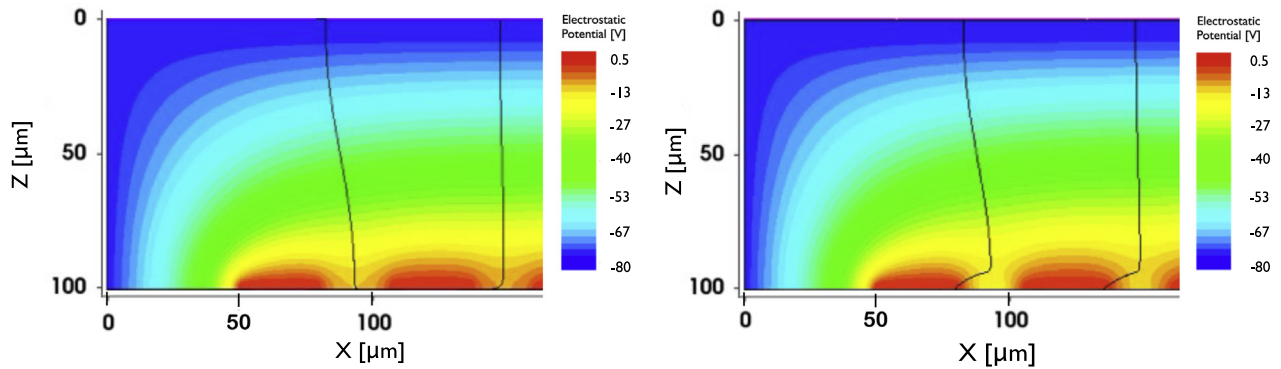

Fig. 8. TCAD simulations of the electrostatic potential of a 100 μm thick n-on-p (left) and n-on-n (right) sensor, both with a 50 μm PTE and operating at −80 V. For both sensor types, the streamlines at the edge are closer to perpendicular than the ones in Fig. 4 (right).

resembles a parallel plate configuration where the edge is relatively far away from the one but last pixel.[8]

---

[8] The comparison to a parallel plate configuration is of limited use when the sensor is mildly overdepleted since in that case the electric field is not constant as a function of Z.

7. Bias dependence on the electric field lines at the edge

The electric field at the edge as a function of the supplied bias voltage was studied for D07-W0160 and H08-W0171. The shape of the edge streamline was determined by the following procedure: (i) each bin of the track coordinate in the charge fraction plots was fitted with a Gaussian, (ii) the mean of each Gaussian was plotted as a function of the X or Y coordinate predicted by the telescope and (iii) the plot was fitted with a second order polynomial.
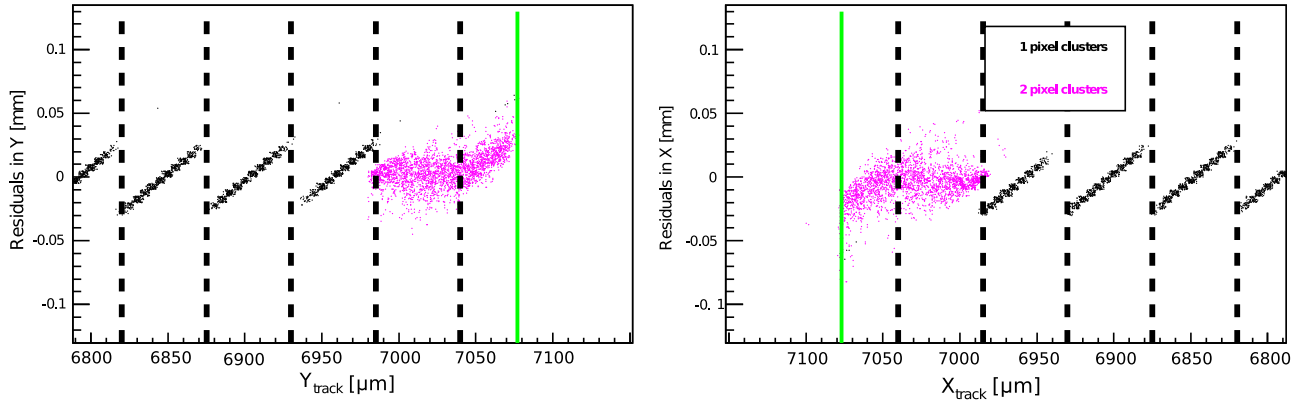
Fig. 9. Residuals in Y as a function of the Y coordinate predicted by the telescope (left) and residuals in X as predicted for the X coordinate (right) for the 150 μm thick n-on-n sensor D07-W0160 with 50 μm PTE after applying the correction in the CoG method. The residuals of the edge two-pixel clusters are not larger than the one-pixel cluster residuals.

For different bias voltages the shape of the streamlines of the electric field at the edge of the 150 μm thick sensor (D07-W0160) does not change significantly as shown in Fig. 7 (left). For the 200 μm thick sensor with the floating GR (H08-W0171) in Fig. 7 (right), the shape of electric field streamlines shows a strong dependence on the applied bias voltage. At -40 V bias, perpendicular tracks beyond 7.04 mm will form two-pixel clusters since the electric field streamlines (purple line) have the usual distorted pattern extending from the boundary of the last two electrodes up to the physical edge. Increasing the bias voltage results in a significant change of the electric field pattern. The edge streamlines become steeper and extend up to the bias side of the sensor (blue line) leading to the formation of one-pixel clusters beyond the boundary of the last pixel.

8. Simulations

Simulations in TCAD provide us with an internal view of the electric field pattern in the sensor. The simulated pattern of the electric field lines at the edge of the 150 μm n-on-n sensor in Fig. 4 (right) is in good agreement with the streamlines obtained from the charge ratio of the edge pixels shown in Fig. 5 (middle left). Additional simulations of a 100 μm thick sensor with a 50 μm PTE sensor were made to investigate the behaviour at the edge. As depicted in Fig. 8 (left), the streamlines at the edge are expected to be closer to perpendicular compared to the case of the 150 μm thick sensor with the 50 μm PTE due to the fact that in this last case the physical edge is further away. This is confirmed by the charge ratio measurement of the J08-W0171 sensor shown in Fig. 5 (top left).

From the sensors of Table 1, both sensors with the minimum distorted edge streamlines (J08-W0171 and C07-W0171) are of sensor type n-on-p. To exclude that the reduction of this distortion is due to the sensor type, sensors with geometries same as J08-W0171 and C07-W0171 but of opposite bulk type were simulated. In Fig. 8 simulations of a sensor with the same geometry as J08-W0171 in n-on-p (left) and in n-on-n configuration (right) show that the distortion of the edge streamlines is independent of the sensor type for highly overdepleted sensors.

9. Corrections on the cluster position at the edge

Using the information from the charge ratios, a better estimate of the cluster position at the edge can be achieved. The spatial

resolution of a pixel or strip detector for one-pixel clusters is pitch/$\sqrt{12}$.[9] This so-called binary resolution can be improved in the case of multi-hit clusters by applying the CoG method mentioned in Section 3 or by applying other corrections such as the eta-function [9]. A similar correction in the CoG of the last two columns (rows) is applied in order to improve the spatial resolution at the edge.

By plotting the cluster coordinates predicted by the telescope as a function of the CoG information from the DUT a correlation function between the two quantities is derived. This correlation function (a second order polynomial) is used to correct the cluster positions beyond 6.98 mm. In Fig. 9 the residuals using the corrected cluster position are plotted for the 150 μm thick sensor (D07-W0160). The distribution of the two-pixel cluster residuals up to the end of the pixel matrix is similar to that of one-pixel clusters. The charge ratio of the two-pixel clusters is uniform beyond the boundary of the last pixel up to the physical edge therefore no correction in the COG position can be applied. The corrections on the cluster position in Fig. 9 are made for perpendicular tracks. The correction function at the edge (similar to the eta function) depends on the angle of the track. One could also apply a correction to the cluster position for angled tracks if an indication of the track angle is given.

10. Conclusions and outlook

The performance at the edge of a novel type of active-edge sensors from VTT using a high precision telescope with a pointing resolution below 2 μm is reported. All sensors are $\sim$100% efficient through all the pixel matrix and > 99% efficient up to 10 μm from the physical edge. A known feature of these active-edge sensors is the distorted pattern of the electric field at the edge. By studying the charge fractions of the edge two-pixel clusters a reconstruction of the streamlines is possible. These reconstructed streamlines are in good agreement with TCAD simulations. The formation of two-pixel clusters at the edge can be used to improve the spatial resolution at the edge of the sensor after applying a correction function. The studies presented should also be made with irradiated sensors. This was however not possible with the Timepix as this ASIC is not radiation hard. Recently the Timepix3 ASIC has become available allowing us to repeat these studies as a function of radiation dose.

---

[9] The measured σ of the resolution is smaller than pitch/$\sqrt{12}$ due to the fact that one-pixel clusters are formed in the center of the pixel.

Acknowledgements

References

[1] V. Fadeyev, et al., Nuclear Instruments and Methods in Physics Research Section A 731 (2013) 260.

[2] C.J. Kenney, et al., Nuclear Instruments and Methods in Physics Research Section A 565 (2006) 272.

[3] X. Wu, et al., JINST 7 (2012) C02001.

[4] K. Akiba, et al., The Timepix Telescope for High Performance Particle Tracking, arXiv:1304.5175v1 [physics.ins-det].

[5] X. Llopart, Design and Characterization of 64 K Pixels Chips Working in Single Photon Processing Mode, CERN-THESIS-2007-062, 2007.

[6] K. Akiba, et al., Nuclear Instruments and Methods in Physics Research Section A 661 (2012) 31.

[7] M.J. Bosma, Active-Edge planar silicon sensors for large-area pixel detectors, in: IEEE Nuclear Science Symposium Conference Record, 2011, pp. 1329–1333.

[8] Synopsys TCAD, ⟨http://www.synopsys.com/tools/tcad/⟩.

[9] E. Belau, et al., Nuclear Instruments and Methods in Physics Research 214 (1983) 253.

[10] J. Jakubek, et al., Nuclear Instruments and Methods in Physics Research Section A 563 (2006) 254.